



Thermal decomposition and kinetics of electrically controlled solid propellant through thermogravimetric analysis

Zhicheng He¹ · Zhixun Xia¹ · Jianxin Hu² · Likun Ma¹ · Yang Li¹

Received: 28 February 2019 / Accepted: 19 July 2019 / Published online: 29 July 2019
© Akadémiai Kiadó, Budapest, Hungary 2019

Abstract

The thermal decomposition behavior of electrically controlled solid propellant (ECSP) with hydroxyl ammonium nitrate as oxidizer and polyvinyl alcohol as binder was investigated through thermogravimetric analysis and differential scanning calorimetry coupling technology at the heating rates of 15, 20, 25, 30, and 35 K min⁻¹ in nitrogen. Results indicated that the T_{initial} and T_{max} values of the thermal decomposition of ECSP increase with heating rates. The activation energy E_a from the results of TG data at various heating rates was calculated by model-free isoconversional Flynn–Wall–Ozawa (FWO) and Kissinger–Akahira–Sunose (KAS) methods. The activation energies obtained through the FWO method were close to those obtained through the KAS method, and the values for activation energy were located between 42.82 and 48.49 kJ mol⁻¹. An appropriate reaction mechanism conversion model for ECSP was determined by Málek and Coats–Redfern methods. Thermal decomposition kinetics of the ECSP obeyed the random nucleation and subsequent growth model, called Avrami–Erofeev function.

Keywords Solid propellant · Thermogravimetric analysis · Activation energy · Kinetic model

Introduction

Hydroxyl ammonium nitrate (HAN, NH₃OHNO₃) has the advantages of low toxicity, high density, high specific impulse, and low freezing point [1–3]. It is recognized as an important ingredient in liquid gun and rocket propellant [4, 5] and considered the main oxidizer and solvent for electrically controlled solid propellant (ECSP) given its electrical conductivity and solubility. ECSPs are a composition that can be ignited by applying electrical voltage and extinguished by withdrawing electrical voltage. Propellant burning rates may be increased/throttled by changing the electrical power supplied [6–8]. In addition, the main gas species of HAN-based ECSP combustion are nitrogen, water, and carbon dioxide, which is eco-friendly [9]. Allowing for the above-mentioned advantages, ECSPs

have been applied in altitude control, rocket booster, missile defense, and space propulsion ignition systems [10–13]. However, several features of the decomposition process of ECSPs hinder their electronic controllability. For example, under certain circumstances, an ECSP can melt or soften during combustion; therefore, it does not extinguish as quickly as desired after the electrical current has stopped [14]. Thus, knowing the thermal decomposition process and kinetic parameters of HAN-based ECSP is necessary to develop an effective electrically controlled propulsion system. However, no data on the kinetics of the thermal decomposition of this compound are available.

The thermal decomposition of solid propellants is a complex process of various physicochemical reactions. Research on the thermal decomposition of solid propellants provides improved insights into the reaction kinetics and mechanisms. Thermogravimetric analysis (TG) and differential scanning calorimetry (DSC) are powerful systems for investigating something more descriptive such as the whole decomposition process of energetic material by increasing the temperature and evaluating its thermal properties. On this basis, information on activation energy and kinetic models can be estimated [15–18]. Shaw and

✉ Zhicheng He
398579983@qq.com

¹ College of Aerospace Science and Engineering, National University of Defense Technology, Changsha 410073, China

² College of Aerospace Engineering, Chongqing University, Chongqing 400044, China

Williams [19] obtained the activation energy in the range from 61 to 71 kJ mol⁻¹ and a pre-exponential factor (*A*) in the range of 3.05×10^{10} – 4.94×10^{10} s⁻¹ for HAN-H₂O mixtures (5.2–9.1 M solutions). Rafeev and Rubtsov [20] obtained an activation energy (*E_a*) of 64 kJ mol⁻¹ for thermal decomposition of a solid HAN. Schoppelrei and Brill [21] used lumped first-order reaction model to simulate the decomposition of HAN. They proposed that the activation energy of HAN decomposition depends on the aqueous solution concentration. Esparza et al. [22] examined the thermal decomposition of aqueous HAN solution (24 mass% HAN) using thermogravimetric analysis instrument with first-order kinetics assumed. They concluded that the activation energy and pre-exponential factor is 62.2 ± 3.7 kJ mol⁻¹ and 2.24×10^4 s⁻¹, respectively. Model fitting and model-free (isoconversional method) are the main methods of thermodynamic research. In the model method, knowing the kinetic model in advance and then obtaining the kinetic parameters using the model is necessary. However, an appropriate reaction model is difficult to acquire in advance. The isoconversional method can provide activation energy values without the necessity of knowing the kinetic model as the kinetic parameter is determined as a function of the degree of conversion, and this method does not suggest a direct evaluation of the pre-exponential factor or kinetic model [23]. However, the isoconversional method can provide an effective compromise between the oversimplified single-step Arrhenius kinetic treatments and the prevalent occurrence of multi-step dynamic processes. For example, the Flynn–Wall–Ozawa (FWO) and Kissinger–Akahira–Sunose (KAS) methods have been widely used for kinetic analysis of the pyrolysis process of different fuels, including coal and fermented cornstalk [24], marine macroalga [25], explosives [26], and composite solid propellants [27].

In the present study, the thermal decomposition behavior of HAN-based ECSP is studied through the TG–DSC in a non-isothermal environment. The kinetic parameter, namely, activation energy, is discussed through Flynn–Wall–Ozawa and Kissinger–Akahira–Sunose methods in detail, and the mechanism function is acquired through Málek and Coats–Redfern methods using non-isothermal TG data. These results are helpful for the understanding of HAN-based ECSP thermal decomposition processes and can provide important references for improving ECSPs.

Materials and methods

Materials

HAN was prepared via a double decomposition reaction between hydroxylammonium sulfate (HAS) and barium

nitrate. The resulting solution was concentrated to make high condensed HAN/water liquid. Then, the dichloromethane–ethyl alcohol solvent was added with stirring. The solid HAN was manufactured after the mixture was cooled at –15 °C. Polyvinyl alcohol (PVA) was purchased from Sigma-Aldrich Co., Ltd. The average relative molecular mass and hydrolysis of the polymer are 146,000–186,000 and 99 + %, respectively. Ammonium nitrate (AN) was purchased from Sigma-Aldrich Co., Ltd. HAN was used as the main oxidizer, and PVA was used as the binder. AN was added to HAN to increase the oxygen content of the propellant and decrease the freezing point of HAN. In preparing the propellant, PVA was first crushed and washed with alcohol to remove impurities. PVA was then dried. The purified PVA was heated for 4 h at 120 °C. HAN was weighed proportionally and added to a glass container. The PVA was added in batches under agitation and the mixture was stirred under a vacuum for 1 h at 25 °C. Finally, a solid propellant was acquired after the mixture was placed in a 50 °C oven for 6–8 days. The formulation of HAN-based ECSP is summarized in Table 1.

Thermogravimetric analysis

The thermal decomposition of each sample was analyzed by TG–DSC coupling technology. Experiments were carried out on a STA 449F3 thermal analyzer (Netzsch, Germany). The mass changes of samples with the temperature over the course of the pyrolysis reaction were measured and recorded. All the samples were placed in an Al₂O₃ crucible, and the sample masses for all the experiments were obtained in the range of 2–3 mg. The experiments were conducted under non-isothermal conditions and heated from 300 K to 775 K at different heating rates (15, 20, 25, 30, and 35 K min⁻¹) under a nitrogen atmosphere at a flow rate of 100 mL min⁻¹.

Kinetic model

KAS and FWO models

The kinetics of heterogeneous decomposition of a solid-state substance can be investigated through the TG, and the

Table 1 Formulation of electrically controlled solid propellant prepared with HAN

Materials	mass%
S-HAN-5 ^a	85
PVA	15

^aHAN/AN = 95/5 by mass

reaction rate is described optimally by the basic kinetic equation [28, 29]:

$$\frac{d\alpha}{dt} = k(T) \cdot f(\alpha) \quad (1)$$

where α is the extent of conversion, t is the time, T is the absolute temperature, $k(T)$ is the reaction rate constant, and $f(\alpha)$ is the reaction model, which is a function of α . The reaction rate constant is typically described in accordance with the Arrhenius equation, which is a function of T and expressed as

$$k(T) = A \exp\left(-\frac{E}{RT}\right) \quad (2)$$

where A is the pre-exponential factor, E is the activation energy, and R is the gas constant. For non-isothermal TG, the degree of conversion for a certain temperature $\alpha(T)$ is described using the following equation [30, 31]:

$$\alpha(T) = \frac{m_0 - m_t}{m_0 - m_\infty} \quad (3)$$

where m_0 , m_t , and m_∞ represent the initial mass, the mass at time t , and the final mass of the samples, respectively. The combination of Eqs. (1) and (2) yields:

$$\frac{d\alpha}{dt} = A \exp\left(-\frac{E}{RT}\right) \cdot f(\alpha) \quad (4)$$

For a dynamic TG in a non-isothermal experimental condition, the function of heating rate is described as follows:

$$T = T_0 + \beta t \quad (5)$$

where T_0 is the initial temperature, t is the time, and β is the heating rate. The rate of conversion, $d\alpha/dt$, for the TG experiment at a constant rate of temperature change, $\beta = dT/dt$, may be expressed as

$$\frac{d\alpha}{dT} = \frac{A}{\beta} \exp\left(-\frac{E}{RT}\right) f(\alpha) \quad (6)$$

$$G(\alpha) = \int_0^\alpha \frac{d\alpha}{f(\alpha)} = \frac{A}{\beta} \int_{T_0}^T \exp\left(-\frac{E_\alpha}{RT}\right) dT \quad (7)$$

where $G(\alpha)$ is the integrated form of the conversion dependence function $f(\alpha)$.

Flynn–Wall–Ozawa (FWO) method

The FWO method is a model-free method; the reaction mechanism may not be considered when using this method. The FWO method is proposed using the following equation [32, 33]:

$$\ln(\beta) = \ln\left(\frac{0.0048AE_\alpha}{RG(\alpha)}\right) - 1.0516 \frac{E_\alpha}{RT} \quad (8)$$

where β is the heating rate, and T is the temperature (in Kelvin) at conversion α . E_α is activation energy (in kJ mol^{-1}) at different α . E_α can be obtained from the slope of the plot of $\ln(\beta)$ versus $1000/T$.

Kissinger–Akahira–Sunose (KAS) method

The KAS method is also a model-free method, which is based on the following equation [34]:

$$\ln\left(\frac{\beta}{T^2}\right) = \ln\left(\frac{AR}{E_\alpha G(\alpha)}\right) - \frac{E_\alpha}{RT} \quad (9)$$

The plot $\ln(\beta/T^2)$ versus $1000/T$ data points obtained from curves recorded at several heating rates must be a straight line. The slope is used to compute the activation energy E_α .

Málek method

When the activation energy E_α is known, the probable mechanism function can be obtained through the Málek method [35–37]. In the case of correlation coefficients close to one another, the Málek method is an effective method. The standard curve equation of the mechanism function can be written as

$$y(\alpha) = \frac{f(\alpha)G(\alpha)}{f(0.5)G(0.5)} \quad (10)$$

The experimental curve equation can be written as

$$y(\alpha) = \left(\frac{T}{T_{0.5}}\right) \frac{\left(\frac{d\alpha}{dt}\right)}{\left(\frac{d\alpha}{dt}\right)_{0.5}} \quad (11)$$

$G(\alpha)$ and $f(\alpha)$ are the theoretical mechanism functions. Several reaction models [38] using $G(\alpha)$ and $f(\alpha)$ are listed in Table 2. The standard curves can be obtained by plotting $y(\alpha)$ versus α from various functions $G(\alpha)$. The experimental curve can be obtained by plotting $y(\alpha)$ versus α from the thermal data at several heating rates. If the experimental data are consistent with the data of the standard curve, then the most probable mechanism function can be acquired.

Coats–Redfern method

This method involves the thermal degradation mechanism and assumes that the Arrhenius parameters do not depend on α . The activation energy E_α and pre-exponential factor A for each degradation mechanism can be obtained from the slope and intercept of a plot of $\ln[G(\alpha)/T^2]$ versus $1000/T$.

Table 2 Algebraic expressions for $G(\alpha)$ of solid-state processes

Mechanisms	Symbol	$f(\alpha)$	$G(\alpha)$
<i>Diffusion models</i>			
1D diffusion	D1	$1/2\alpha$	α^2
2D diffusion	D2	$[-\ln(1-\alpha)]^{-1}$	$\alpha + (1-\alpha)\ln(1-\alpha)$
3D diffusion-Jander equation	D3	$(3/2)(1-\alpha)^{2/3}[1-(1-\alpha)^{1/3}]^{-1}$	$[1-(1-\alpha)^{1/3}]^2$
Ginstling–Brounshtein	D4	$(3/2)[(1-\alpha)^{-1/3}-1]^{-1}$	$(3/2)[(1-\alpha)^{-1/3}-1]^{-1}$
Z.-L.-T. equation	3D	$(3/2)(1-\alpha)^{4/3}[(1-\alpha)^{1/3}-1]^{-1}$	$[(1-\alpha)^{1/3}-1]^2$
<i>Nucleation models</i>			
Power law	P2	$2\alpha^{(1/2)}$	$\alpha^{(1/2)}$
Power law	P3	$3\alpha^{(2/3)}$	$\alpha^{(1/3)}$
Power law	P4	$4\alpha^{(3/4)}$	$\alpha^{(1/4)}$
Avrami–Erofeev	A2	$2(1-\alpha)[-\ln(1-\alpha)]^{1/2}$	$[-\ln(1-\alpha)]^{1/2}$
Avrami–Erofeev	A3	$3(1-\alpha)[-\ln(1-\alpha)]^{2/3}$	$[-\ln(1-\alpha)]^{1/3}$
Avrami–Erofeev	A4	$4(1-\alpha)[-\ln(1-\alpha)]^{3/4}$	$[-\ln(1-\alpha)]^{1/4}$
Avrami–Erofeev	$n = 3/2$	$(2/3)(1-\alpha)[-\ln(1-\alpha)]^{1/2}$	$[-\ln(1-\alpha)]^{3/2}$
J-M-A Equation	An	$n(1-\alpha)[-\ln(1-\alpha)]^{1-1/n}$	$[-\ln(1-\alpha)]^{1/n}$
<i>Geometrical contraction models</i>			
Contracting area	R1	1	A
Contracting area	R2	$2(1-\alpha)^{1/2}$	$1-(1-\alpha)^{1/2}$
Contracting area	R3	$3(1-\alpha)^{2/3}$	$1-(1-\alpha)^{1/3}$
<i>Reaction-order models</i>			
First-order	F1	$1-\alpha$	$-\ln(1-\alpha)$
Second-order	F2	$(1-\alpha)^2$	$(1-\alpha)^{-1}-1$
Third-order	F3	$(1-\alpha)^3$	$(1/2)[(1-\alpha)^{-2}-1]$
	F $_n$	$(1-\alpha)^n$	$[(1-\alpha)^{-(n-1)}-1]/(n-1)$
n th order	$n = 1/4$	$4(1-\alpha)^{3/4}$	$1-(1-\alpha)^{1/4}$
2/3 order	/	$2(1-\alpha)^{3/2}$	$(1-\alpha)^{-1/2}$

This method can be described using the following equation [39]:

$$\ln \frac{G(\alpha)}{T^2} = \ln \left(\frac{AR}{\beta E_\alpha} \right) - \frac{E_\alpha}{RT} \quad (12)$$

Results and discussion

Thermal degradation of ECSP

To explore the thermal degradation process of ECSP, the TG, DTG, and DSC were used to investigate the characteristics of ECSPs at five heating rates. Figures 1 and 2 illustrate the TG and DTG curves of ECSPs at different heating rates, respectively. The TG curve of the ECSP in a nitrogen atmosphere at a heating rate of 15 K min^{-1} showed a major change in a mass of 88% in the temperature range of 106–202 °C. The results obtained were similar when the heating rate (β) was changed to 20, 25, 30,

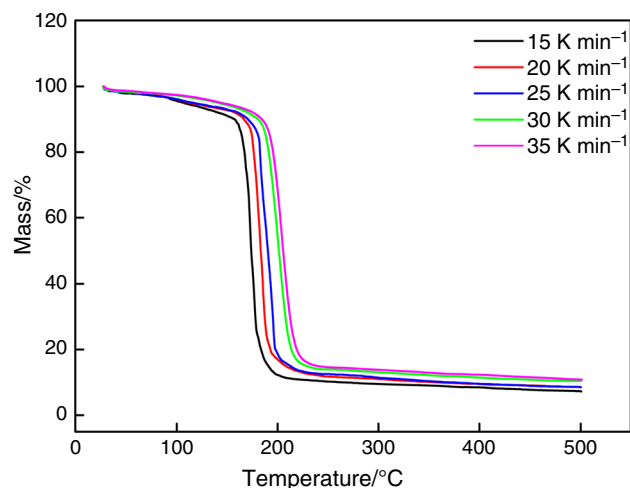


Fig. 1 TG curves of ECSP at different heating rates

and 35 K min^{-1} . When the heating rate was changed to 35 K min^{-1} , an initial mass loss was observed at the high

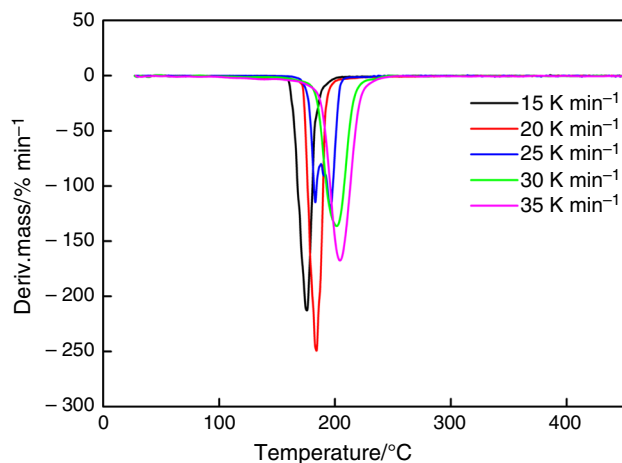


Fig. 2 DTG curves of ECSP at different heating rates

temperature range of 112–144 °C. The DTG curve of the ECSP showed a maximum decomposition rate at 176 °C, 184 °C, 201 °C, and 203 °C at heating rates of 15, 20, 30, and 35 K min⁻¹, respectively. These results indicated that the degradation of ECSP occurs nearly totally in a one-step process as can be concluded by the presence of only one peak in the DTG curve at heating rates of 15, 20, 30, and 35 K min⁻¹. Two peaks emerged in the DTG curve at a 25 K min⁻¹ heating rate; one peak is close to the that of a low heating rate (20 K min⁻¹), and the other peak is close to the that of a high heating rate (30 K min⁻¹). The TG curve showed the main stage. This situation may be a transitional phenomenon from a low to a high heating rate. With the increase in the heating rate from 15 to 35 K min⁻¹, the T_{initial} of the TG and T_{max} of the DTG curve shifted to the positive side of the horizontal coordinate axis for the sample. The lateral shift of the TG and DTG curves of the ECSP could be explained by the following reasons: (1) The shape of the DTG changes with the heating rate change from low heating rates (15 and 20 K min⁻¹) to high heating rates (30 and 35 K min⁻¹), thereby indicating that the mechanism of the thermal decomposition of the ECSP may have changed for changing the heating rate affects the product distribution of HAN by altering the rates of the various competitive decomposition reactions [40]. (2) The shorter time was required to reach a certain temperature at higher heating rate, and there existed a temperature gradient from the outer surface and the inner core of the propellant. A high heating rate indicates a considerable gradient. By contrast, the internal and external temperatures of the propellant are relatively small at low heating rates. Therefore, considering the combined effects of the heat transfer at different heating rates and the kinetics of the decomposition that results in delayed decomposition, the displacement of the curves can be observed [15, 25, 41]. The DSC curves are illustrated in Fig. 3. Only

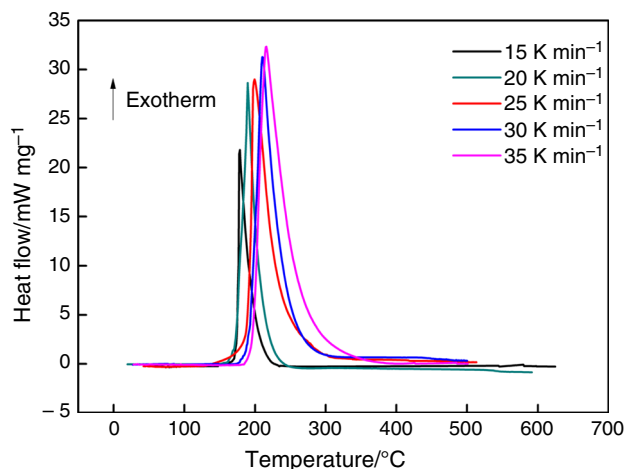


Fig. 3 DSC curves of ECSP at different heating rates

one exothermic peak at various heating rates was observed in the DSC curves of HAN-based ECSP. This peak was due to the thermal decomposition of the propellant. The exothermic peaks showed a remarkable dependency on the heating rate. The temperature of the decomposition peaks increased with the heating rate given the dependence of the conversion degree (α) on time and temperature [42].

Calculation of the activation energy

Activation energy E_{α} is considered the minimum energy required for a chemical reaction to occur. For calculating the activation energy, the isoconversional FWO and KAS methods were used to determine the activation energy because the mechanism function of the thermal decomposition of the ECSP does not require being known in advance. In the FWO method, the plot of $\ln(\beta)$ versus $1000/T$ should be a straight line, and the activation energies were calculated at different conversion rates ($0.1 \leq \alpha \leq 0.9$) in accordance with Eq. (8). In the KAS method, the activation energy could also be calculated at different conversion rates ($0.1 \leq \alpha \leq 0.9$) on the basis of the slope by plotting $\ln(\beta/T^2)$ versus $1000/T$ in accordance with Eq. (9).

Figures 4 and 5 depict the dependence of activation energy on the conversion for $\alpha = 0.1$ – 0.9 for the ECSP based on the isoconversional FWO and KAS methods, correspondingly. Table 3 lists the values of activation energy E_{α} and standard deviations calculated through the FWO and KAS methods. In Table 3, the R^2 of all curves ranged from 0.9783 to 0.9977, thereby indicating that all linear plots demonstrate favorable correlation. The relatively small standard deviations for E_{α} implied that the activation energies obtained were close for both considered methods. The FWO yields a slightly higher value (i.e., 60.29–52.28 kJ mol⁻¹) than the 55.95–44.80 kJ mol⁻¹

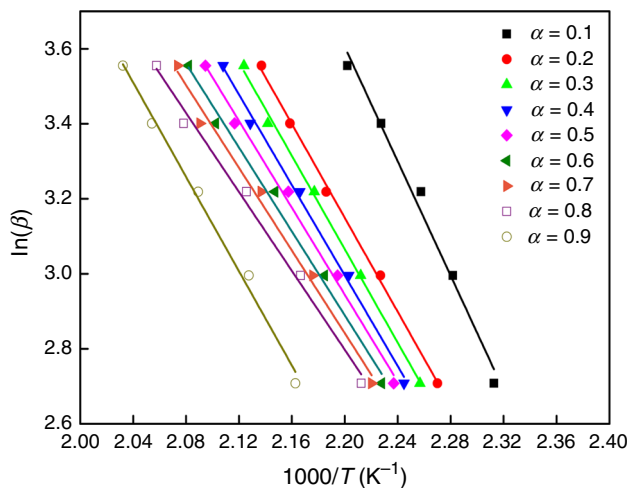


Fig. 4 FWO plots of ECSP at different heating rates

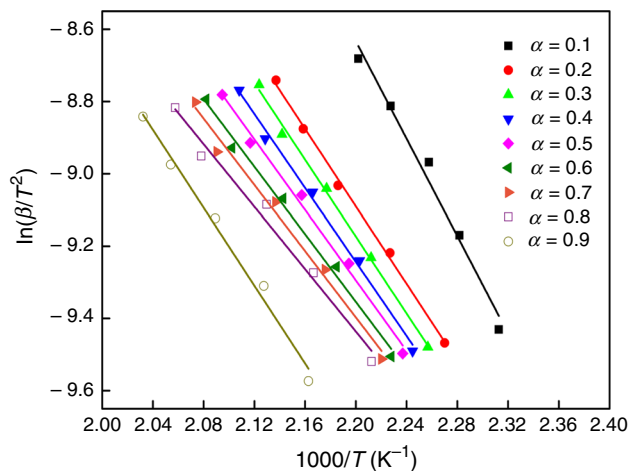


Fig. 5 KAS plots of ECSP at different heating rates

obtained through the KAS method. The average value of the E_α of the ECSP was 48.49 and 42.82 kJ mol^{-1} through the FWO and the KAS methods, respectively. The mean activation energy calculated through the two methods is

Table 3 Activation energies of ECSP obtained by FWO and KAS methods

α	FWO		KAS		Average
	$E_\alpha/\text{kJ mol}^{-1}$	R^2	$E_\alpha/\text{kJ mol}^{-1}$	R^2	
0.1	60.29 ± 1.50	0.9832	55.95 ± 1.60	0.9783	58.12 ± 1.55
0.2	49.50 ± 0.68	0.9977	44.48 ± 0.82	0.9969	46.99 ± 0.75
0.3	49.25 ± 0.48	0.9969	44.23 ± 0.46	0.9957	46.74 ± 0.47
0.4	47.73 ± 0.59	0.9951	42.55 ± 0.65	0.9931	45.14 ± 0.62
0.5	45.84 ± 0.33	0.9933	40.52 ± 0.31	0.9902	43.18 ± 0.32
0.6	44.25 ± 0.76	0.9897	38.85 ± 0.74	0.9896	41.55 ± 0.75
0.7	43.60 ± 1.03	0.9882	38.10 ± 1.02	0.9827	40.85 ± 1.03
0.8	43.69 ± 1.75	0.9897	35.89 ± 1.96	0.9771	39.79 ± 1.86
0.9	52.28 ± 2.24	0.9913	44.80 ± 1.44	0.9856	48.54 ± 1.84
Average	48.49 ± 1.04		42.82 ± 1.00		45.66 ± 1.02

approximate, thereby indicating that the results have favorable reliability. The deviation in the average E_α values for the ECSP between the KAS and FWO methods was 6.21%; the E_α values between 42.82 and 48.50 kJ mol^{-1} could be acceptable.

Figure 6 plots the relationship between the average activation energy E_α calculated through the FWO and KAS methods at different conversions. The E_α value at 0.1 conversion is the maximum, thereby indicating that high energy is required in the initial stage of the reaction. With the development of chemical reaction, the E_α value decreases from 46.99 to 39.79 kJ mol^{-1} with the increase in conversion ratio from 0.2 to 0.8. However, the E_α value rises to 48.54 kJ mol^{-1} when the conversion ratio increases from 0.8 to 0.9, thus denoting that the degree of difficulty in reaction increased at 0.9 or higher conversion.

Determination of the degradation mechanism

The theoretical curves $y(\alpha)$ versus α is plotted using Eq. (10) on the basis of the different reaction mechanisms $G(\alpha)$ summarized in Table 2. This situation occurs because, when $a \leq 0.1$ or $a \geq 0.9$, the reaction is in the initial or finished stage, and the activation energies are much higher than that at the conversion ratio of 0.2–0.8; the initial and finished stage of the reaction cannot represent the whole process of reaction. Thus, we selected the reaction stage with a conversion ratio of 0.2–0.8 for studying the thermal decomposition mechanism of the ECSP. The experiment curves are plotted using Eq. (11) on the basis of the TG data at the conversion ratio of 0.2–0.8, which are from the TG curves at heating rates of 15, 20, 30, and 35 K min^{-1} . In this study, the conversion range of the temperature was within 0.2–0.8. Figure 7 displays the $y(\alpha)$ versus α theoretical and experimental curves of the ECSP, respectively. Figure 7 presents that the experimental curves of the ECSP could not fit well with the theoretical curves.

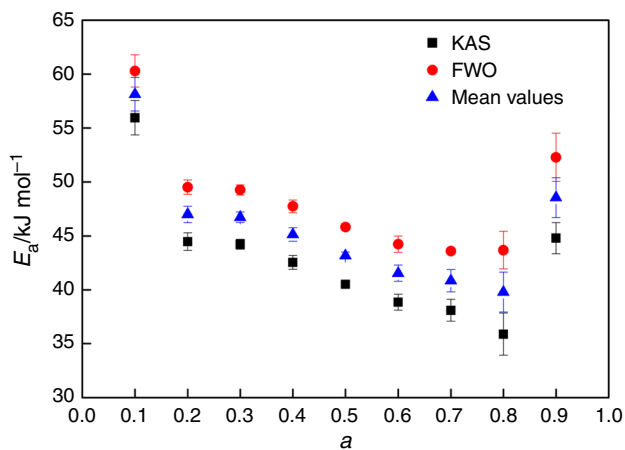


Fig. 6 Dependence of E_{α} on α for non-isothermal data evaluated by FWO and KAS methods

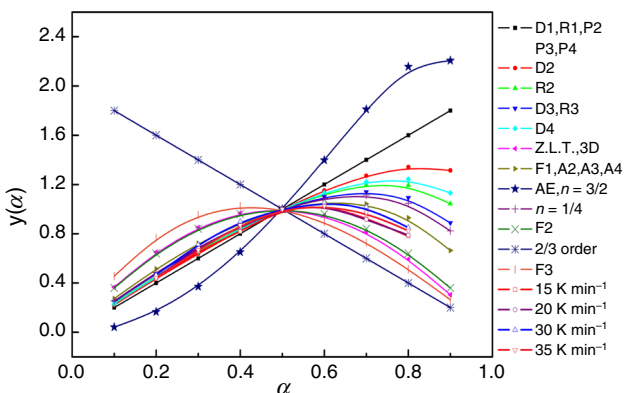


Fig. 7 Masterplots of different kinetic models and experimental data at 15, 20, 30, and 35 K min⁻¹ calculated by Eq. (11) for ECSP thermal degradation

Nevertheless, the experimental curves are close to the theoretical curves of A2, A3, and A4, and the experimental curves are also located between the theoretical curves of F1 and F2. This result indicated that the An and Fn functions may be suitable for describing the thermal decomposition process of the ECSP. However, determining the type of mechanism that is most suitable requires further research.

The Coats–Redfern method is an extensively used procedure for determining the reaction processes. To acquire a relatively optimal thermal decomposition mechanism of the ECSP, the Coats–Redfern method was used further to determine the thermal degradation mechanism of the ECSP. Combined with 11 types of mechanism functions of An ($n = 2-4$) and Fn ($n = 1-2$), the corresponding values of E_{α} , A, and R^2 obtained through the Coats–Redfern method were obtained. Furthermore, the values of E_{α} determined through the FWO and KAS methods were used to restrict the E_{α} value of the above-mentioned results. In

Table 4 Activation energies of ECSP in nitrogen atmosphere obtained by Coats–Redfern method

	15/K min ⁻¹			20/K min ⁻¹			30/K min ⁻¹			35/K min ⁻¹		
	E_{α} /kJ mol ⁻¹	lnA/min ⁻¹	R^2	E_{α} /kJ mol ⁻¹	lnA/min ⁻¹	R^2	E_{α} /kJ mol ⁻¹	lnA/min ⁻¹	R^2	E_{α} /kJ mol ⁻¹	lnA/min ⁻¹	R^2
A2	131.32 ± 8.54	34.59 ± 2.25	0.9963	129.25 ± 5.58	34.31 ± 1.81	0.9974	92.75 ± 1.51	23.80 ± 7.26	0.9947	93.96 ± 5.58	24.03 ± 1.76	0.9915
A3	85.02 ± 5.68	22.00 ± 1.53	0.9960	83.64 ± 3.74	21.91 ± 1.25	0.9972	59.21 ± 1.00	14.89 ± 7.03	0.9942	60.00 ± 3.89	15.09 ± 1.33	0.9907
A4	61.88 ± 4.28	15.61 ± 1.17	0.9956	60.85 ± 2.83	15.61 ± 0.98	0.9970	42.44 ± 0.74	10.32 ± 6.85	0.9936	43.01 ± 2.90	10.51 ± 1.11	0.9897
A5	48.86 ± 3.79	12.25 ± 1.17	0.9992	47.16 ± 2.26	11.76 ± 0.81	0.9968	32.38 ± 0.60	7.51 ± 6.70	0.9930	32.83 ± 2.33	7.69 ± 0.99	0.9911
A6	38.72 ± 2.83	9.06 ± 0.81	0.9952	38.03 ± 1.91	9.15 ± 0.71	0.9966	25.77 ± 0.52	5.59 ± 6.58	0.9922	26.04 ± 1.93	5.76 ± 0.91	0.9875
F1	273.76 ± 18.74	74.19 ± 5.43	0.9992	266.07 ± 11.12	70.94 ± 3.47	0.9975	193.35 ± 3.11	49.94 ± 0.94	0.9952	195.84 ± 11.76	50.25 ± 3.10	0.9922
F1.2	293.48 ± 19.83	79.65 ± 5.75	0.9987	285.44 ± 11.79	76.20 ± 3.69	0.9985	207.67 ± 3.25	53.74 ± 0.97	0.9972	210.36 ± 12.57	54.06 ± 3.29	0.9943
F1.4	314.30 ± 21.01	85.41 ± 6.08	0.9974	305.89 ± 12.53	81.75 ± 3.92	0.9986	222.78 ± 3.38	57.74 ± 1.01	0.9982	225.68 ± 13.40	58.08 ± 3.48	0.9954
F1.6	336.17 ± 22.23	91.45 ± 6.44	0.9953	327.38 ± 13.34	87.58 ± 4.17	0.9979	238.69 ± 3.53	61.94 ± 1.05	0.9983	241.79 ± 14.36	62.30 ± 3.70	0.9956
F1.8	359.11 ± 23.52	97.78 ± 6.80	0.9926	349.91 ± 14.19	93.68 ± 4.42	0.9964	255.37 ± 3.70	66.34 ± 1.10	0.9976	258.69 ± 15.30	66.71 ± 3.92	0.9950
F2	383.04 ± 24.85	104.38 ± 7.19	0.9894	373.45 ± 15.09	100.05 ± 4.70	0.9944	272.77 ± 3.85	70.93 ± 1.16	0.9964	276.33 ± 16.32	71.32 ± 4.15	0.9938

Table 5 Kinetic parameters and decomposition equations obtained by Coats–Redfern method

Heating rates/K min ⁻¹	E_{α} /kJ mol ⁻¹	lnA/min ⁻¹	R^2	Decomposition equation
15–20	48.01 ± 1.20	12.01 ± 0.35	0.9968–0.9992	$dz/dt = 0.82 \times 10^6 \exp(-4.80 \times 10^4/RT)(1 - \alpha)[- \ln(1 - \alpha)]^{4/5}$
30–35	42.73 ± 0.40	10.42 ± 0.13	0.9897–0.9936	$dz/dt = 0.13 \times 10^6 \exp(-4.27 \times 10^4/RT)(1 - \alpha)[- \ln(1 - \alpha)]^{3/4}$

accordance with Eq. (12), Coats and Redfern proposed the kinetic parameters calculated by this method at varying heating rates, as listed in Table 4. In the present study, the same conversion values as those used in the Málek method were used. An A5 reaction type provides the optimal straight line, with which a high correlation coefficient of a linear regression analysis at low heating rates (15 and 20 K min⁻¹) was observed. The activation energy calculated at 15 and 20 K min⁻¹ heating rates using the slopes of A5 was 48.86 and 47.16 kJ mol⁻¹, correspondingly. For high heating rates (30 and 35 K min⁻¹), the mechanism for ECSP degradation was proposed to be the A4 type. The activation energy calculated for the heating rates of 30 and 35 K min⁻¹ was 42.44 and 43.01 kJ mol⁻¹, respectively. The above-mentioned results indicated that the E_{α} value obtained through the Coats–Redfern method is close to the activation energy (42.82–48.49 kJ mol⁻¹) obtained through the FWO and KAS isoconversional methods. Simultaneously, the correlation coefficient R^2 was high. The thermal decomposition behavior of the ECSP at 25 K min⁻¹ might contain A4 and A5 reaction types. Therefore, the most probable kinetic mechanism of the ECSP follows a nucleation and growth model called Avrami–Erofeev function. Then, the A4 and A5 functions were used to calculate the pre-exponential factor (A), which was described by $[- \ln(1 - \alpha)]^{1/4}$ and $[- \ln(1 - \alpha)]^{1/5}$, respectively. The average E_{α} and lnA values at the heating rates of 15 and 20 K min⁻¹ were 48.01 kJ mol⁻¹ and 12.01 min⁻¹. The average E_{α} and lnA values at heating rates of 30 and 35 K min⁻¹ were 42.73 kJ mol⁻¹ and 10.42 min⁻¹. Therefore, the order reaction model function $f(\alpha) = 5(1 - \alpha)[- \ln(1 - \alpha)]^{4/5}$ was obtained for low heating rates (15 and 20 K min⁻¹) and $f(\alpha) = 4(1 - \alpha)[- \ln(1 - \alpha)]^{3/4}$ for high heating rates (30 and 35 K min⁻¹). These results indicated that the heating rate has a certain influence on the thermal decomposition mechanism of the HAN-based ECSP. When the heating rate is relatively slow, the order of reaction is higher than that at a high heating rate, thereby suggesting that the reaction is increasingly complicated at this condition. The E_{α} values were lower at high heating rates than at low heating rates, thereby indicating that at such a high heating rate, low activation energy will be required for high conversions given the easy overcoming of mass and heat transfer limitations [28, 43]. The thermal decomposition

reaction equation is obtained using Eq. (4). The results are summarized in Table 5.

Conclusions

The thermal behavior and kinetics of the ECSP were investigated through the TG at five heating rates (15, 20, 25, 30, and 35 min⁻¹), and the decomposition of the ECSP involves approximately 85% loss in mass in the ranges of 112–238 °C. The E_{α} values of the ECSP achieved through the FWO and KAS method were between 42.82 and 48.49 kJ mol⁻¹ in the 0.1–0.9 conversion range. The analyses of the results obtained through the Málek and Coats–Redfern methods in the 0.2–0.8 conversion range showed that the degradation mechanism of the ECSP in N₂ moves to an An mechanism. The pyrolysis reaction models of the ECSP can be described using A5 at the heating rates of 15 and 20 K min⁻¹, whereas that of the ECSP can be described using A4 at the heating rates of 30 and 35 K min⁻¹. The kinetic function differential form of A5 and A4 is $f(\alpha) = 5(1 - \alpha)[- \ln(1 - \alpha)]^{4/5}$ and $f(\alpha) = 4(1 - \alpha)[- \ln(1 - \alpha)]^{3/4}$, correspondingly.

References

1. Chang YP, Boyer E, Kuo KK. Combustion behavior and flame structure of XM46 liquid propellant. *J Propul Power*. 2001;17(4):800–8.
2. Hwang CH, Baek SW, Cho SJ. Experimental investigation of decomposition and evaporation characteristics of HAN-based monopropellants. *Combust Flame*. 2014;161:1109–16.
3. Amrousse R, Katsumi T, Itouyama N, Azuma N, Kagawa H, Hatai K, Ikeda H, Hori K. New HAN-based mixtures for reaction control system and low toxic spacecraft propulsion subsystem: thermal decomposition and possible thruster applications. *Combust Flame*. 2015;162:2686–92.
4. Lee HS, Litzinger TA. Chemical kinetic study of HAN decomposition. *Combust Flame*. 2003;135:151–69.
5. Koh KS, Chin JK, Wahida K, Chik TF. Role of electrodes in ambient electrolytic decomposition of hydroxylammonium nitrate (HAN) solutions. *Propul Power Res*. 2013;2(3):194–200.
6. Dulligan M, Lake J, Adkison P, Spanjers G, White D, Nguyen H. Methods of controlling solid propellant ignition, combustion, and extinguishment. 2010; U.S. Patent 7770380.
7. Sawka WN. Family of metastable intermolecular composites utilizing energetic liquid oxidizers with nanoparticle fuels in sol-gel polymer network. 2011; U.S. Patent 2011/0030859.

8. Grix CE, Sawka WN. Family of modifiable high performance electrically controlled propellants and explosives. 2011; U.S. Patent 20110067789.
9. Sawka W, McPherson M. Electrical solid propellants: a safe, micro to macro propulsion technology. In: 49th AIAA/ASME/SAE/ASEE joint propulsion conference and exhibit; 2013.
10. Dulligan M, Lake J, Adkison P, Spanjers G, White D, Nguyen H. Electrically controlled extinguishable solid propellant motors. 2008; U.S. Patent 20080092521.
11. Sawka WN, Grix C. Electrode ignition and control of electrically ignitable materials. 2014; U.S. Patent 8857338.
12. Duchemin O, Yvart PM. Space vehicle with electric propulsion and solid propellant chemical propulsion. 2015; U.S. Patent 20150021439.
13. Mcpherson MD. Electrically ignited and throttled pyroelectric propellant rocket engine. 2015; U.S. Patent 20150059314.
14. Katzakian A, Grix C. High performance electrically controlled solution solid propellant. 2012; U.S. Patent 8317952.
15. Wang QF, Wang L, Zhang XW, Mi ZT. Thermal stability and kinetic of decomposition of nitrated HTPB. *J Hazard Mater.* 2009;172:1659–64.
16. Li XT, Li HQ, Liu HT, Zhu GY. Non-isothermal thermal decomposition reaction kinetics of dimethylhexane-1,6-dicarbamate (HDC). *J Hazard Mater.* 2011;198:376–80.
17. Yi JH, Zhao FQ, Wang BZ, Liu Q, Zhou C, Hu RZ, Ren YH, Xu SY, Xu KZ, Ren XN. Thermal behaviors, nonisothermal decomposition reaction kinetics, thermal safety and burning rates of BTATz-CMDB propellant. *J Hazard Mater.* 2010;181:432–9.
18. Zhang JQ, Gao HX, Su LH, Hu RZ, Zhao FQ, Wang BZ. Non-isothermal thermal decomposition reaction kinetics of 2-nitroimino-5-nitro-hexahydro-1,3,5-triazine (NNHT). *J Hazard Mater.* 2009;167:205–8.
19. Shaw BD, Williams FA. A model for the deflagration of aqueous solutions of hydroxylammonium nitrate. *Symp (Int) Combust.* 1992;24:1923–30.
20. Rafeev VA, Rubtsov YI. Kinetics and mechanism of thermal decomposition of hydroxylammonium nitrate. *Russ Chem Bull.* 1993;42:1811–901.
21. Schoppelrei JW, Brill TB. Spectroscopy of hydrothermal reactions. 7. Kinetics of aqueous $[\text{NH}_2\text{OH}]\text{NO}_3$ at 463–523K and 27.5 MPa by infrared spectroscopy. *J Phys Chem A.* 1997;101:8593–6.
22. Esparza AA, Ferguson RE, Choudhuri A, Love ND, Shafirovich E. Thermoanalytical studies on the thermal and catalytic decomposition of aqueous hydroxylammonium nitrate solution. *Combust Flame.* 2018;193:417–23.
23. López-Fonseca R, Landa I, Gutiérrez-Ortiz MA, González-Velasco JR. Non-isothermal analysis of the kinetic of the combustion of carbonaceous materials. *J Therm Anal Calorim.* 2005;80:65–9.
24. He YY, Chang C, Li P, Han XL, Lia HL, Fang SQ, Chen JY, Ma XJ. Thermal decomposition and kinetics of coal and fermented cornstalk using thermogravimetric analysis. *Bioresour Technol.* 2018;259:294–303.
25. Das P, Mondal D, Maiti S. Thermochemical conversion pathways of *Kappaphycus alvarezii* granules through study of kinetic models. *Bioresour Technol.* 2017;234:233–42.
26. Singh A, Sharma TC, Kumar M, Narang JK, Kishore P, Srivastava A. Thermal decomposition and kinetics of plastic bonded explosives based on mixture of HMX and TATB with polymer matrices. *Defence Technol.* 2017;13:22–32.
27. Trache D, Maggi F, Palmucci I, DeLuca LT. Thermal behavior and decomposition kinetics of composite solid propellants in the presence of amide burning rate suppressants. *J Therm Anal Calorim.* 2018;132:1601–15.
28. Sell T, Vyazovkin S, Wight CA. Thermal decomposition kinetics of PBAN-binder and composite solid rocket propellants. *Combust Flame.* 1999;119:174–81.
29. Trache D, Abdelaziz A, Siouani B. A simple and linear isoconversional method to determine the pre-exponential factors and the mathematical reaction mechanism functions. *J Therm Anal Calorim.* 2017;128:335–48.
30. Rajić M, Sućeska M. Study of thermal decomposition kinetics of low-temperature reaction of ammonium perchlorate by isothermal TG. *J Therm Anal Calorim.* 2001;63:375–86.
31. Xiao HM, Ma XQ, Lai ZY. Iso-conversional kinetic analysis of co-combustion of sewage sludge with straw and coal. *Appl Energy.* 2009;86:1741–5.
32. Ozawa T. A new method of analyzing thermogravimetric data. *Bull Chem Soc Jpn.* 1965;38:1881–6.
33. Flynn JH, Wall LA. A Quick direct method for the determination of activation energy from thermogravimetric data. *Polym Lett.* 1966;4:323–8.
34. Kissinger HE. Reaction kinetics in differential thermal analysis. *Anal Chem.* 1957;29:1702–6.
35. Mále J. A compute program for kinetic analysis of non-isothermal thermoanalytical data. *Thermochim Acta.* 1989;138:337–46.
36. Mále J, Smrčka V. The kinetic analysis of the crystallization processes in glasses. *Thermochim Acta.* 1991;186:153–69.
37. Mále J. The kinetic analysis of non-isothermal data. *Thermochim Acta.* 1992;200:257–69.
38. Khawam A, Flanagan DR. Role of isoconversional methods in varying activation energies of solid-state kinetics II. Non-isothermal kinetic studies. *Thermochim Acta.* 2005;436:101–12.
39. Coats AW, Redern JP. Kinetic parameters from the thermogravimetric data. *Nature.* 1964;201:68.
40. Cronin JT, Brill TB. Thermal decomposition of energetic materials. 8. Evidence of an oscillating process during the high-rate thermolysis of hydroxylammonium nitrate, and comments on the interionic interactions. *J Phys Chem.* 1986;90:178–81.
41. Maiti S, Purakayastha S, Ghosh B. Thermal characterization of mustard straw and stalk in nitrogen at different heating rates. *Fuel.* 2007;86:1513–8.
42. Zhang GZ, Zhang J, Wang F, Li HJ. Thermal decomposition and kinetics studies on the poly (2,2-dinitropropyl acrylate) and 2,2-dinitropropyl acrylate-2,2-dinitrobutyl acrylate copolymer. *J Therm Anal Calorim.* 2015;122:419–26.
43. Haykiri-Acma H, Yaman S, Kucukbayrak S. Effect of heating rate on the pyrolysis yields of rapeseed. *Renew Energ.* 2006;31:803–10.

Publisher's Note Springer Nature remains neutral with regard to jurisdictional claims in published maps and institutional affiliations.